Spatial Metabolomics Identifies Distinct Tumor-Specific Subtypes in Gastric Cancer Patients

Jun Wang[1], Thomas Kunzke[1], Verena M. Prade[1], Jian Shen[1], Achim Buck[1], Annette Feuchtinger[1], Ivonne Haffner[2], Birgit Luber[3], Drolaiz H.W. Liu[4,5], Rupert Langer[5], Florian Lordick[2,6], Na Sun[1], and Axel Walch[1]

ABSTRACT

Purpose: Current systems of gastric cancer molecular classification include genomic, molecular, and morphological features. Gastric cancer classification based on tissue metabolomics remains lacking. This study aimed to define metabolically distinct gastric cancer subtypes and identify their clinicopathological and molecular characteristics.

Experimental Design: Spatial metabolomics by high mass resolution imaging mass spectrometry was performed in 362 patients with gastric cancer. K−means clustering was used to define tumor and stroma-related subtypes based on tissue metabolites. The identified subtypes were linked with clinicopathological characteristics, molecular features, and metabolic signatures. Responses to trastuzumab treatment were investigated across the subtypes by introducing an independent patient cohort with HER2-positive gastric cancer from a multicenter observational study.

Results: Three tumor- and three stroma-specific subtypes with distinct tissue metabolite patterns were identified. Tumor-specific subtype T1(HER2$^+$MIB$^+$CD3$^+$) positively correlated with HER2, MIB1, DEFA-1, CD3, CD8, FOXP3, but negatively correlated with MMR. Tumor-specific subtype T2(HER2$^-$MIB$^-$CD3$^-$) negatively correlated with HER2, MIB1, CD3, FOXP3, but positively correlated with MMR. Tumor-specific subtype T3(pEGFR$^+$) positively correlated with pEGFR. Patients with tumor subtype T1(HER2$^+$MIB$^+$CD3$^+$) had elevated nucleotide levels, enhanced DNA metabolism, and a better prognosis than T2 (HER2$^-$MIB$^-$CD3$^-$) and T3(pEGFR$^+$). An independent validation cohort confirmed that the T1 subtype benefited from trastuzumab therapy. Stroma-specific subtypes had no association with clinicopathological characteristics, however, linked to distinct metabolic pathways and molecular features.

Conclusions: Patient subtypes derived by tissue-based spatial metabolomics are a valuable addition to existing gastric cancer molecular classification systems. Metabolic differences between the subtypes and their associations with molecular features could provide a valuable tool to aid in selecting specific treatment approaches.

Introduction

Gastric cancer is a leading cause of cancer-related deaths with the fourth highest mortality rate worldwide (1). Treatment responsiveness of gastric cancer differs markedly among current therapeutic regimens (2). To improve gastric cancer stratification for clinical practice, research focuses on developing classification systems based on multiple molecular levels, such as genome, transcriptome, and proteome, to identify novel predictive biomarkers for personalized gastric cancer treatment (3, 4).

Several recent studies have provided a molecular subtyping framework, including morphological, genomic, and proteomic features, to draw a roadmap for gastric cancer drug development and personalized therapy (5, 6). Two comprehensive, large-scale studies from the Cancer Genome Atlas (TCGA) Research Network in 2014 and the Asian Cancer Research Group (ACRG) Network in 2015 are among these molecular classification systems. TCGA characterized the gastric cancer genome and proteome using complex bioinformatics analysis of array-based somatic copy number, whole-exome sequencing, array-based DNA methylation profiling, messenger ribonucleic acid sequencing, microRNA sequencing and reverse-phase protein array data. The TCGA study identified four genomic subtypes: Epstein–Barr virus–positive (EBV$^+$) tumors, microsatellite instable (MSI) tumors, genomically stable tumors, and tumors with chromosomal instability. Another large-scale study by the ACRG established four molecular subtypes using the gene expression, genome-wide copy-number microarray and targeted sequencing: MSS/EMT subtype, MSI subtype, MSS/TP53-active subtype, and MSS/TP53-inactive subtype (7, 8).

Gastric cancer could be considered potentially immunogenic. Several other studies characterized gastric cancer with immunological features (9, 10). Li and colleagues (9) identified three subtypes using a newly proposed pathway-based gastric cancer classification method: Immune-derived subtype (ImD), stroma-enriched subtype, and immune-enriched subtype and Zeng and colleagues (10) defined three gastric cancer subtypes based on patterns of immune cell infiltration into the tumor microenvironment.

The development of practical classification systems to predict treatment responses in patients with gastric cancer would be a valuable

[1]Research Unit Analytical Pathology, Helmholtz Zentrum München—German Research Center for Environmental Health, Neuherberg, Germany. [2]University Cancer Center Leipzig (UCCL), Leipzig University Medical Center, Leipzig, Germany. [3]Technische Universität München, Fakultät für Medizin, Klinikum rechts der Isar, Institut für Allgemeine Pathologie und Pathologische Anatomie, München, Germany. [4]Department of Pathology, GROW School for Oncology and Reproduction, Maastricht University Medical Center, Maastricht, the Netherlands. [5]Institute of Clinical Pathology and Molecular Pathology, Kepler University Hospital and Johannes Kepler University, Linz, Austria. [6]Department of Oncology, Gastroenterology, Hepatology, Pulmonology and Infectious Diseases, Leipzig University Medical Center, Leipzig, Germany.

Note: Supplementary data for this article are available at Clinical Cancer Research Online (http://clincancerres.aacrjournals.org/).

Corresponding Authors: Axel Walch, Ingolstädter Landstraße 1, Neuherberg, 85764, Germany. Phone: 49 89 3187-3349; E-mail: axel.walch@helmholtz-muenchen.de; and Na Sun, na.sun@helmholtz-muenchen.de

Clin Cancer Res 2022;XX:XX–XX

doi: 10.1158/1078-0432.CCR-21-4383

Translational Relevance

In recent years, several gastric cancer molecular classification systems have been established. However, gastric cancer classification based on metabolomics is still lacking. Here, we developed a novel tumor- and stroma-specific classification model to stratify a large series of patients with gastric cancer by applying tissue-based spatial metabolomics combined with K−means clustering analysis. Using this model, all of tumor- and stroma-specific subtypes were strongly associated with molecular features and distinctive metabolism pathways. Application of an independent validation cohort revealed that two tumor-specific subtypes were predictive of trastuzumab response. This is the first study to stratify patients with gastric cancer based on tissue metabolomics. Metabolic differences of the patient subtypes and their associations with molecular features could improve the personalization of therapeutic regimens.

addition to clinic settings. For example, trastuzumab represents the first option for approximately 20% of patients with HER2 overexpression (11). The MSS/TP53-inactive molecular subtype established by the ACRG study has been reported to potentially benefit from anti–HER2-directed therapy (8). The immunotherapeutic antibody, pembrolizumab, selectively binds to programmed cell death protein 1 (PD-1; ref. 12) and several clinical studies have correlated EBV infection and MSI status with PD1/PD-L1 blockade (13, 14). The high response and benefit of microsatellite instability-high (MSI-H) patient subtypes to PD-L1 blockade therapy is another example of how personalized treatment can benefit specific patient subgroups based on molecular features (15). Interestingly, the tendency to have a lymphocytic infiltrate, which is observed in MSI tumors, likely reflects immune activation of T cells that are associated with MSI (16, 17). Furthermore, one study extended to four surface markers of tumor-infiltrating lymphocytes (TIL), including cluster of differentiation 8 (CD8), cluster of differentiation 4 (CD4), PD-1, and forkhead box P3 (FOXP3) in patients with gastric cancer (18). Thus, identification of these multiple molecular markers, together with their molecular classifications, opens novel perspectives to stratify patients who may benefit from immune and targeted therapies.

Metabolism reprogramming is a hallmark of cancer. To meet the growing energy demands required for cell proliferation, gastric cancer cells have a unique metabolism comprising glucose, glutamine, fatty acids, amino acids, and many other nutrients and metabolites, such as glycolysis, repressed aerobic respiration, and *de novo* fatty acid synthesis (19–21). The recent deep exploration of molecular changes induced by rewired metabolism has led to the development of targeted therapies (22, 23). Indeed, a previous study identified several metabolite-dependent subtypes among 33 cancer types (24). Metabolite-level classification has not been comprehensively investigated in gastric cancer; hence, we assessed the ability of metabolite profiles to stratify patients with gastric cancer and explored the association with clinical molecular features.

High mass resolution Matrix-assisted laser desorption-ionization (MALDI) imaging mass spectrometry (IMS) directly enables detection and localization of thousands of different molecules within a routinely preserved tissue section, and thus greatly facilitates the application of MALDI-IMS for tumor subtyping (25–27). Recently, a new computational multimodal workflow, Spatial Correlation Image Analysis (SPACiAL), which designed to combine molecular imaging data with multiplex IHC, was developed for an objective analysis of high-throughput data from large-scale clinical cohort studies (28).

This study aimed to derive a novel classification scheme to stratify patients with gastric cancer by their metabolic profiles, encompass clinicopathological characteristics and molecular feature correlation, and more importantly, assign clinical treatment relevance to patient subtypes. High mass resolution MALDI-IMS combined with K−means clustering analysis was applied to establish metabolic classification based on tumor- and stroma-specific tissue regions in patients with gastric cancer. The results were validated in an independent validation cohort to demonstrate the predictive metabolic constitution of the subtypes for the trastuzumab therapy. The metabolic constitution in gastric cancer provided an alternative for patient stratification.

Patients and Methods

Collection of tissue samples and clinical characteristics data

Primary resected gastric cancer samples were obtained from 362 patients who had not received prior chemotherapy, trastuzumab therapy, or immunotherapy. Tissue microarrays (TMA) were analyzed in triplicates (three tissue cores from each patient; **Table 1**). All samples used in this study were obtained from patients who underwent gastrectomy between 1995 and 2005 at the Surgery Department at the Technical University Munich. This study was conducted in accordance with the Declaration of Helsinki, and approved by the local Ethics Committee of the Faculty of Medicine at Technical University Munich with informed written consent from all patients. **Table 1** describes the clinical characteristics of the gastric cancer participants. Pathological TNM-staging was performed according to the Union Internationale Contre le Cancer (UICC) system 7th edition (29) and histopathological grading was classified in accordance to the World Health Organization (30). Parameter variables were categorized as follows: Sex into female versus male; tumor node metastasis classification, pT1–pT4 for primary tumor, pN0–pN3 for primary lymph nodes, M0 and M1 category for distant metastasis; UICC classification into stage I–stage IV; resection state into R0–R2; Lauren classification into diffuse, intestinal, and mixed type; and primary tumor grading into scores of G1–G3.

Patients and tissue samples for the independent validation cohort (VARIANZ cohort)

A previous publication established a metabolomic classifier to predict trastuzumab therapy response in patients with HER2-positive advanced gastric cancer (VARIANZ cohort; ref. 31). The VARIANZ cohort data were integrated here as a validation study for predicting trastuzumab therapy response of the metabolic subtypes. The VARIANZ cohort ($n = 42$) was divided into therapy-resistant ($n = 17$) and therapy-sensitive ($n = 25$) patients (31). This study was conducted in accordance with the Declaration of Helsinki, and approved by the Ethics Committee of the Leipzig University Medical Faculty with informed written consent from all patients (32). The patients were centrally reviewed, and their HER2 status was fully characterized by the application of IHC staining and ISH. All patients included in this analysis belonged to UICC stage IV, were HER2-positive and underwent trastuzumab therapy and chemotherapy (platin-fluoropyrimidine; Supplementary Table S1).

Sample acquisition and preparation

Sample preparation was performed as previously described (26). Briefly, formalin-fixed paraffin-embedded sections (3 μm, Microm,

Q5 **Table 1.** Summary of patient characteristics.

Characteristic	Numbers
Number of patients	362
Age, y	
Median	68
Range	17–100
Sex	
Male	219
Female	123
NA	20
Survival time (mo)	
Median	20
Range	0–344
NA	108
Lauren classification	
Intestinal	178
Diffuse	146
Mixed	15
NA	23
Primary tumor extension	
pT1	40
pT2	140
pT3	134
pT4	28
NA	20
Regional lymph nodes	
pN0	93
pN1	100
pN2	107
pN3	35
NA	27
Distant metastasis	
M0	193
M1	82
NA	87
UICC stage	
Stage I	87
Stage II	71
Stage III	77
Stage IV	105
NA	22
Primary resection state	
R0	203
R1	78
R2	29
NA	52
Grade	
G1	2
G2	48
G3	285
NA	27

Note: Distant metastasis was defined as metastasis in any lymph node other than regional. Samples with insufficient data to make a conclusion were set to "NA."

HM340E, Thermo Fisher Scientific) were mounted onto indium–tin–oxide-coated glass slides (Bruker Daltonik) pretreated with 1:1 poly-L-lysine (Sigma-Aldrich) and 0.1% Nonidet P-40 (Sigma). Deparaffinized tissue sections were spray-coated with 10 mg/mL of 9-aminoacridine hydrochloride monohydrate matrix (Sigma-Aldrich) in 70% methanol using a SunCollect sprayer (Sunchrom).

High mass resolution MALDI-Fourier transforms ion cyclotron resonance IMS

High mass resolution MALDI-IMS was conducted as previously described (26). MALDI-IMS was performed in negative ion mode using a Bruker Solarix 7.0 T FT-ICR (Fourier transforms ion cyclotron resonance) MS (Bruker Daltonik) equipped with a dual ESI-MALDI source and a SmartBeam-II Nd: YAG (355 nm) laser. Data acquisition parameters were specified in ftmsControl software 2.2 and flexImaging (v. 5.0; Bruker Daltonik). Mass spectra were acquired covering m/z 50–1100. The laser operated at a frequency of 1000 Hz, using 100 laser shots per pixel, and with a pixel resolution of 60 μm. Non-tissue regions were measured as a background control to differentiate between tissue and matrix-associated peaks. L-Arginine was used for external calibration in the ESI mode. After MALDI-IMS analysis, the matrix was removed with 70% ethanol, and the samples were stained with hematoxylin and eosin (H&E), coverslipped, and scanned with an AxioScan.Z1 digital slide scanner (Zeiss) equipped with a ×20 magnification objective.

Multiplex fluorescent IHC staining

TMAs were analyzed by double staining for pan-cytokeratin [monoclonal mouse pan-cytokeratin plus (AE1/AE3þ8/18; 1:75), catalog no. CM162, Biocare Medical, RRID: AB_10582491] and vimentin [recombinant anti-vimentin antibody (EPR3776; 1:500), catalog no. ab92547, Abcam, RRID: AB_10562134]. Signal was detected using fluorescence-labeled secondary antibodies [goat anti-rabbit IgG (H + L)-cross-adsorbed secondary antibody-DyLight 633 (1:200), catalog no. 35563; and goat anti-mouse IgG (H + L)-cross-adsorbed secondary antibody-Alexa Fluor 750 (1:100), catalog no. A-21037, RRID: AB_2535708, both Thermo Fisher Scientific]. Nuclei were identified with Hoechst 33342 in all stains. Fluorescence stains were scanned with an AxioScan.Z1 digital slide scanner (Zeiss) equipped with a ×20 magnification objective and visualized with ZEN 2.3 blue edition software (Zeiss).

IHC and ISH

Protein expression of molecular features, including HER2, DNA mismatch repair (MMR), phospho-EGFR (pEGFR), E3 ubiquitin-protein ligase (MIB1), cluster of differentiation 3 (CD3), CD8, FOXP3, and human alpha defensin 1 (DEFA-1), *HER2* ISH status and Epstein–Barr virus (EBV) positivity, were performed as pre-viously described (33, 34). In short, IHC with anti-HER2/neu (A0785; 1:300, DAKO), anti-pEGFR (36-9700; 1:100, Invitrogen, RRID: AB_2533287), anti-CD3 (RM-9107-S; 1:200; Thermo Fisher Scientific, RRID: AB_149922), anti-CD8 (ab178089; 1:50, Abcam, RRID: AB_2756374), anti–DEFA-1 (T1034; 1:400, Dioanova), anti-FOXP3 (12653; 1:100, Cell Signaling Technology), and anti-MIB1 (M7240; 1:100, DAKO, RRID: AB_2142367) were performed on consecutive 3-μm sections using an automated stainer (Ventana DISCOVERY XT System, Ventana Medical Systems, Inc.) according to the manufacturer's instructions. Antibodies mutL homolog 1 (MLH1; clone ES05, Agilent Dako, RRID: AB_2631352) and mutS homolog 2 (MSH2; clone FE11, Biocare Medical) of the DNA MMR proteins were stained on consecutive 3-μm sections (BenchMark ULTRA System). An assay with fluorescence-labeled locus-specific DNA probes for *HER2* and chromosome-17 (CEP17) centromeric α-satellite was hybridized onto TMAs for ISH analysis. The TMAs were incubated with an EBV-encoded small RNA probe (DAKO Cytomations) for EBV-encoded small RNA ISH analysis.

Immunophenotype-guided IMS and data processing

In situ tissue cores were processed using the SPACiAL pipeline for immunophenotype-guided MALDI-IMS analysis, which includes a series of MALDI data and image-processing steps to automatically annotate tumor and stroma regions as previously described (28). First, H&E staining was removed by incubating tissue sections with 70% ethanol for 5 minutes followed by IHC. Tumor and stroma regions were distinguished by multiplex fluorescent IHC staining with epithelial cell–specific cytokeratin antibody [(AE1/AE3þ8/18; 1:75), catalog no. CM162, Biocare Medical, US, RRID: AB_10582491] and stroma cell–specific vimentin antibody [recombinant anti-vimentin antibody (EPR3776; 1:500), catalog no. ab92547, Abcam, UK, RRID: AB_10562134] on the same tissue section. Immunostaining images were then co-registered with the MALDI measurement region to define 347 tumor region samples and 339 stroma region samples by SPACiAL workflow. Specification of tumor and stroma regions and exportation of each patient's spectral data were finally managed using the SPACiAL pipeline (28).

Consensus clustering

Consensus clustering was conducted using the "ConcensusClusterPlus" package in R to explore gastric cancer subtypes based on the cancer patient sample matrix. The consensus matrix was used to check cluster co-occurrence, find intrinsic groupings over variation in different numbers of clusters, and use K−means on the distance matrix. The matrix is arranged so that samples belonging to the same cluster are adjacent to each other.

Pathway enrichment analysis

Metabolites were annotated with the Kyoto Encyclopedia of Genes and Genomes (KEGG, RRID: SCR_012773; www.genome.jp/kegg/), allowing M−H, M−H_2O, M+K−2H, M+Na−2H, and M+Cl as negative adducts with a mass tolerance of 4 ppm. Significance analysis of tumor- or stroma-specific subtypes was performed by a Kruskal–Wallis test with subsequent Benjamini–Hochberg correction ($P < 0.05$). The enriched metabolites in each subtype were identified by comparing with every other subtype using the Dunn's test with a cutoff P value of <0.05 and a fold change of >1 based on the significant metabolites. The feature matrix of enriched metabolites was then normalized by the 0–1 normalization method, which scaled the minimum of each row to zero and maximum to one as visualized by the abundance heatmap. Pathway enrichment analysis was performed via the KEGG database (RRID: SCR_012773) using the MetaboAnalyst online tool (RRID: SCR_015539; www.metaboanalyst.ca; Fisher's exact test, $q < 0.05$ for FDR correction).

Statistical analysis

Correlations were calculated using pairwise Spearman's rank-order correlation and P values were adjusted with Benjamini–Hochberg correction. The clinicopathological characteristics differences among tumor- and stroma-specific subtypes was evaluated by the χ^2 test or Fisher's exact test, and P values in the pairwise comparison between subtypes were adjusted with FDR correction. To determine the intensity differences of representative metabolites, the Kruskal–Wallis and *post hoc* Dunn's multiple comparison tests were used in conjunction with Benjamini–Hochberg correction. The Mann–Whitney U test was used for testing intensity differences in the validation cohort. Further statistical differences and comparison in patient survival were determined using the Kaplan–Meier curve and the Log–Rank test. Multivariate survival analysis was performed using Cox proportional hazard regression model. All statistical tests were conducted using R (R version 4.0.0, RRID: SCR_001905).

Data availability

The data generated in this study are available upon reasonable request from the corresponding author.

Results

Identification of gastric cancer patient subtype based on metabolite profiling

The study workflow is shown in **Fig. 1**. From a total of 362 patient samples, 347 could be automatically annotated with tumor regions and 339 could be annotated with stroma regions using immuno-guided spatial metabolomics. The annotatable patient cases form the basis for our calculations. To determine whether tumor and stroma regions had significantly different metabolite compositions, we performed a tumor and stroma region-specific unsupervised K−means clustering analysis. A total of 9,278 ion features were identified and selected as the basis of K−means clustering.

Consensus matrix heatmaps and cumulative distribution function (CDF) plots were drawn to determine the optimal number of K clusters. Optimal cluster numbers for tumor-specific and stroma-specific data were both set to 3, which led to a lesser increase in CDF difference following the consensus index (**Fig. 2A** and **B**). Color-coded heatmaps corresponding to the consensus matrix were obtained by applying consensus clustering to tumor- and stroma-specific datasets (**Fig. 2C** and **D**). The selected blocks were almost disjointed in the heatmap, indicating that the three clusters could be distinguished on tumor-specific spectra. The three clusters also had relatively clean separation and displayed a well-defined three-block structure for stroma-specific data. The sharp and crisp boundaries further validated stable and robust clustering of the tumor- and stroma-specific dataset. Both datasets were subsequently processed by unsupervised K−means centroid clustering. Of the 347 tumor regions, 161 were assigned to subtype T1 (46%), 55 to T2 (16%), and 131 to T3 (38%), respectively. Furthermore, of the 339 stroma regions, 125 were assigned to subtype S1 (37%), 50 to subtype S2 (15%), and 164 to subtype S3 (48%).

To estimate the ability of MALDI-IMS data to distinguish gastric cancer subtypes and validate subtype assignments without referring to clustering, we additionally assessed the variance among molecular subtypes using a t-distributed stochastic neighbor embedding-based approach. Results showed that both tumor- and stroma-specific subtypes were clearly separated, indicating that they could be readily distinguished on the basis of metabolite levels (**Fig. 2E** and **F**).

Correlation of tumor- and stroma-specific subtypes with molecular features

To explore differences in tumor- and stroma-specific subtypes, we investigated their association with molecular features, including DNA MMR, HER2, pEGFR, E3 ubiquitin-protein ligase (MIB1), CD3, CD8, FOXP3, and human alpha defensin 1 (DEFA-1), *HER2* ISH status, and EBV positivity. All associations between molecular features and patient subtypes are shown in **Fig. 2G–H** and Supplementary Tables S2 and S3. Among the three tumor-specific subtypes, gastric cancer molecular features, including HER2 ($P = 0.00017$), CD3 ($P = 0.005$), CD8 ($P = 0.02$), FOXP3 ($P = 0.0011$), MIB1 ($P = 0.0012$), and DEFA-1 ($P = 0.014$) positively correlated with tumor-specific subtype T1. Conversely, pEGFR ($P = 0.012$) and MMR ($P = 0.0033$) negatively correlated with T1. Tumor-specific subtype T2 negatively correlated with

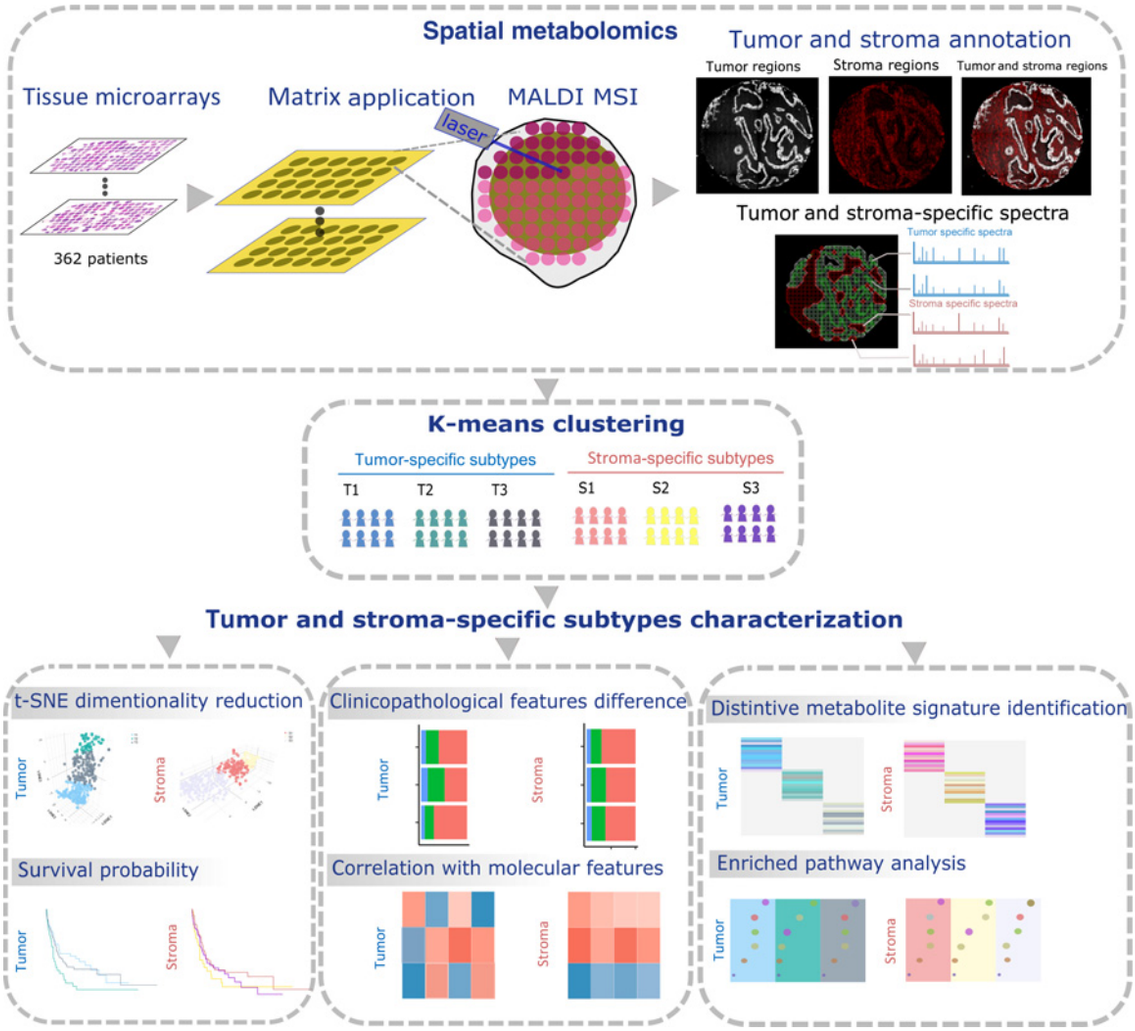

Figure 1.

Spatial metabolomics pipeline scheme and subtype characterization process. The workflow begins with immunophenotype-guided spatial metabolomics, including matrix application, immunophenotype-guided MALDI-IMS assessment, and data processing. For the immunophenotype-guided MALDI-IMS approach, tumor and stroma cells were annotated using multiplex fluorescent IHC staining. Tumor and stroma region-specific mass spectra were then subjected to further the K−means clustering and statistical analysis.

HER2 ($P = 0.0076$), CD3 ($P = 0.017$), FOXP3 ($P = 0.0013$), and MIB1 ($P = 0.00009$). Meanwhile, T2 showed no significant correlation with CD8 ($P = 0.13$), DEFA-1 ($P = 0.080$), and pEGFR ($P = 0.89$). Conversely, MMR ($P = 0.047$) positively correlated with T2. Tumor-specific subtype T3 positively correlated with pEGFR ($P = 0.013$) and showed no significant correlation with HER2 ($P = 0.082$), MMR ($P = 0.17$), CD3 ($P = 0.23$), CD8 ($P = 0.23$), FOXP3 ($P = 0.36$), MIB1 ($P = 0.71$), and DEFA-1 ($P = 0.26$). The metabolic subtypes significantly correlated with HER2 IHC status, but showed no correlation with *HER2* ISH status. As shown in Supplementary Table S4, EBV positivity was observed in 14 patients. Of these, 9 and 5 EBV-positive tumors were the T1 and T2 subtype, whereas no EBV-positive tumor samples were the T2 subtype. On the basis of these results, we categorized tumor-specific subtypes based on HER2, MIB1, and CD3-positive correlation as T1 ($HER2^{+}MIB^{+}CD3^{+}$), those based on negative HER2, MIB1, and CD3 correlation, as T2($HER2^{-}MIB^{-}CD3^{-}$), and the remaining tumor subtype based on elevated pEGFR protein expression, as T3 ($pEGFR^{+}$).

Stroma-specific subtype S1 did not significantly correlate with HER2 ($P = 0.098$), MMR ($P = 0.572$), pEGFR ($P = 0.49$), MIB1 ($P = 0.21$), DEFA-1 ($P = 0.20$), CD3 ($P = 0.22$), or CD8 ($P = 0.51$), and indeed had a negative correlation with FOXP3 ($P = 0.028$). Stroma-specific subtype S2 was negatively associated with HER2 ($P = 0.028$), MIB1 ($P = 0.002$), FOXP3 ($P = 0.002$), and CD3 ($P = 0.019$). Meanwhile, S2 did not significantly correlate with MMR ($P = 0.0847$), pEGFR ($P = 0.14$), DEFA-1 ($P = 0.47$), or CD8 ($P = 0.22$). Stroma-specific subtype S3 had a positive correlation with HER2 ($P = 0.0019$), MIB1 ($P = 0.00079$), FOXP3 ($P = 0.000013$), and CD3 ($P = 0.008$), and had no significant correlation with MMR ($P = 0.5$), pEGFR ($P = 0.11$), DEFA-1 ($P = 0.082$), and CD8 ($P = 0.14$). Of the 14

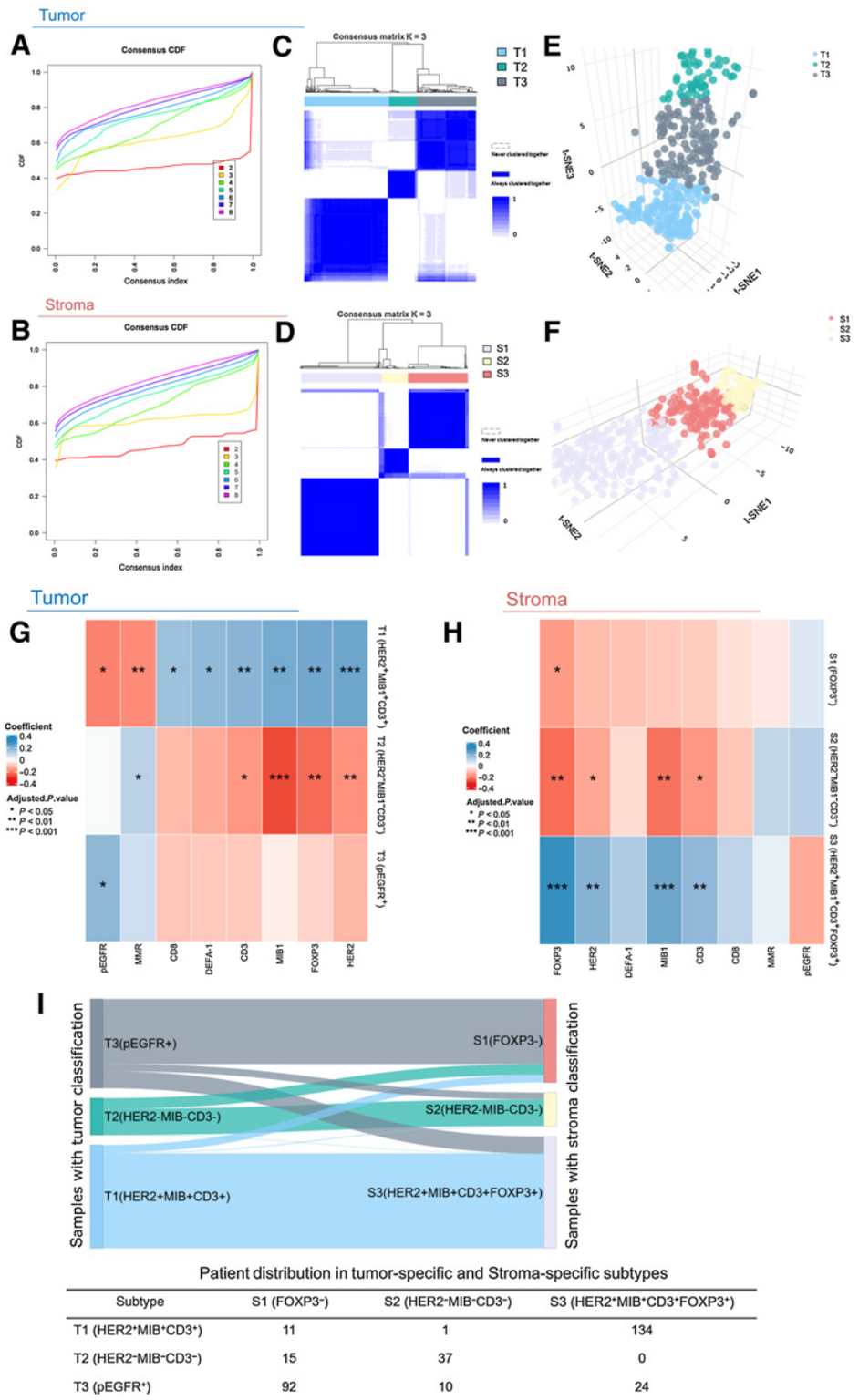

Patient distribution in tumor-specific and Stroma-specific subtypes

Subtype	S1 (FOXP3$^-$)	S2 (HER2$^-$MIB$^-$CD3$^-$)	S3 (HER2$^+$MIB$^+$CD3$^+$FOXP3$^+$)
T1 (HER2$^+$MIB$^+$CD3$^+$)	11	1	134
T2 (HER2$^-$MIB$^-$CD3$^-$)	15	37	0
T3 (pEGFR$^+$)	92	10	24

Figure 2.

Tumor- and stroma-specific subtypes identification and their association with molecular features. The relative change in the area under CDF curve of (**A**) tumor and (**B**) stroma datasets. The number of cluster K changed from 2 to 8. $K = 3$ led to a lesser increase in CDF difference following the consensus index and thus was selected as the optimal number of cluster. Consensus matrix heatmap of the chosen optimal number of cluster $K = 3$ of (**C**) tumor and (**D**) stroma-specific datasets. A color gradient of 0–1 is used, blue = consensus score of 1, meaning that patients were always clustered together; white = consensus score of 0, meaning that patients were never clustered together. Three-dimensional t-SNE analysis supported that patients could be stratified into three subtypes in both tumor- (**E**) and stroma-specific datasets. **F,** Points represented samples colored according to the metabolic patient subtypes. Statistical association of molecular features (HER2, MMR, pEGFR, MIB1, CD3, CD8, FOXP3, and DEFA-1) with tumor- (**G**) and stroma-specific subtypes (**H**). **E,** Alluvial diagram depicted the relationship of tumor- and stroma-specific subtypes. Detailed patient numbers in each subtype were shown in the table; *, $P < 0.05$; **, $P < 0.01$; and ***, $P < 0.001$.

EBV-positive tumors, 3 and 11 EBV-positive tumors were the S1 and S3 subtype, whereas no EBV-positive tumor samples were the S2 subtype (Supplementary Table S4). Hence, stroma-specific subtypes were accordingly named S1(FOXP3$^-$), S2(HER2$^-$MIB$^-$CD3$^-$), and S3(HER2$^+$MIB$^+$CD3$^+$FOXP3$^+$). The alluvial diagram shown in **Fig. 2I** indicated the distribution of patients between tumor- and stroma-specific subtypes. Subtype similarities were observed between T1(HER2$^+$MIB$^+$CD3$^+$) and S3(HER2$^+$MIB$^+$CD3$^+$FOXP3$^+$),

T2(HER2$^-$MIB$^-$CD3$^-$) and S2(HER2$^-$MIB$^-$CD3$^-$), and T3(pEGFR$^+$) and S1(FOXP3$^-$).

Tumor-specific subtypes have different clinicopathological features

We next tested whether consensus clustering subtypes had striking differences in the most common gastric cancer clinicopathological characteristics. Our results showed that the proportion of samples in pT ($P = 0.022$), pN ($P = 0.0043$), M ($P = 0.00017$), and UICC stage ($P = 0.00026$) was significantly different in distinct tumor-specific subtypes (Supplementary Fig. S1D–S1F and S1H). Particularly, T1 (HER2$^+$MIB$^+$CD3$^+$) subtype had a significantly different proportion of samples in the "M stage" in comparison with the T2 (HER2$^-$MIB$^-$CD3$^-$) and T3(pEGFR+) subtypes. No associations of tumor-specific subtypes with age, sex, grade, or Lauren classification were found (Supplementary Fig. S1A, S1B, S1G, and S1I). Stroma-specific subtypes were not significantly associated with clinicopathological characteristics (Supplementary Fig. S1).

Association between tumor-specific subtypes and patient prognosis

We next compared potential differences in prognosis among tumor- and stroma-specific subtypes. The Kaplan–Meier survival analysis indicated better outcomes for subtype T1(HER2$^+$MIB$^+$CD3$^+$) than T2(HER2$^-$MIB$^-$CD3$^-$; $P = 0.022$; **Fig. 3B**). No statistically significant differences were observed in other pairwise tumor-specific subtype comparisons or overall, in three tumor-specific subtype comparisons (**Fig. 3A**, **C**, and **D**). In stroma-specific subtypes, survival was not statistically different in pairwise subtype comparisons or in an overall comparison of the three subtypes (**Fig. 3E–H**). The T1 (HER2$^+$MIB$^+$CD3$^+$) and T2(HER2$^-$MIB$^-$CD3$^-$) subtypes, which have significant survival differences, were included in the multivariate Cox regression analysis, and showed that tumor-specific subtypes do not serve as independent prognostic subtypes with regard to the UICC classification system [T1(HER2$^+$MIB$^+$CD3$^+$): $P = 0.323$; hazard ratio (HR), 1.244; T2(HER2$^-$MIB$^-$CD3$^-$): $P = 0.481$; HR, 1.184; UICC stage: $P = 5.38 \times 10^{-12}$; HR, 1.970].

Gastric cancer patient subtypes with distinct metabolites and related metabolism pathways

To gain a deeper insight into the underlying metabolism differences among tumor- and stroma-specific subtypes, a differential analysis was conducted on 277 annotated metabolites, and significant enriched metabolites for each of tumor- and stroma-specific subtypes were identified. Enriched metabolites for each subtype were visualized by a heatmap as shown in **Fig. 4A** and Supplementary Fig. S2A. **Figure 4B–D** and Supplementary Fig. S2B–S2D separately demonstrated distinct subtype-specific pathway patterns of tumor and stroma. T1 (HER2$^+$MIB$^+$CD3$^+$) had 45 significantly upregulated metabolic pathways, 13 of which were related to carbohydrate metabolism, as opposed to 10 that were related to amino acid metabolism (**Fig. 4B**). Notably, nucleotide metabolism and ascorbate and aldarate metabolism were upregulated exclusively in T1(HER2$^+$MIB$^+$CD3$^+$). At the same time, T2(HER2$^-$MIB$^-$CD3$^-$) had 17 significantly upregulated metabolic pathways, 7 of which were related to carbohydrate metabolism and 4 were related to amino acid metabolism, respectively (**Fig. 4C**). T3 (pEGFR$^+$) was found to be related to biotin metabolism and the cytosolic DNA-sensing pathway (**Fig. 4D**). Concerning stroma-specific subtypes, S3(HER2$^+$MIB$^+$CD3$^+$FOXP3$^+$) had 32 specific upregulated metabolism pathways, in comparison with 2 and 17 in S1(FOXP3$^-$) and S2(HER2$^-$MIB$^-$CD3$^-$), respectively (Supplementary Fig. S2B–S2D). S1(FOXP3$^-$) was related to the pentose phosphate pathway and cysteine and methionine metabolism (Supplementary Fig. S2B). Furthermore, some amino acid-related pathways were elevated in S3(HER2$^+$MIB$^+$CD3$^+$FOXP3$^+$; Supplementary Fig. S2D). **Figure 4E** and Supplementary Fig. S2E showed the spatial distribution of one representative metabolite selected from each tumor- and stroma subtype-specific pathway. The above results demonstrate that tumor- and stroma-specific subtypes were enriched with diverse metabolites and metabolism pathways.

T1(HER2$^+$MIB$^+$CD3$^+$) and T2(HER2$^-$MIB$^-$CD3$^-$) subtypes correlate with trastuzumab therapy efficiency in an independent validation cohort (VARIANZ cohort)

Response to trastuzumab therapy in gastric cancer has been linked to a metabolomic classifier in our recent study (**Fig. 5A** and **B**; ref. 31). This metabolomic classifier was established by applying spatial metabolomics and machine learning. The metabolomic classifier could stratify patients diagnosed with HER2-positive gastric cancer into trastuzumab-sensitive and trastuzumab-resistant, and thus predict those patients' response to trastuzumab. HER2-positive tumor patients from the study were used as an independent validation cohort (VARIANZ cohort), and the metabolomic classifier was applied to predict trastuzumab responses in T1(HER2$^+$MIB$^+$CD3$^+$) and T2(HER2$^-$MIB$^-$CD3$^-$) subtypes, due to their specific correlation with HER2 protein expression. As shown in **Fig. 5C** and **D**, the metabolomic classifier can distinguish T1(HER2$^+$MIB$^+$CD3$^+$) and T2(HER2$^-$MIB$^-$CD3$^-$) subtypes in our discovery cohort. In the VARIANZ cohort ($n = 42$), patients treated with trastuzumab therapy were classified into the T1(HER2$^+$MIB$^+$CD3$^+$) and T2(HER2$^-$MIB$^-$CD3$^-$) subtypes, which significantly correlated with a response to trastuzumab (**Fig. 5E**). The percentage of trastuzumab-sensitive patients was significantly higher in the T1(HER2$^+$MIB$^+$CD3$^+$) subtype (82%) than in the T2 (HER2$^-$MIB$^-$CD3$^-$) subtype (44%; **Fig. 5F**). In addition, trastuzumab-treated patients in the T1(HER2$^+$MIB$^+$CD3$^+$) subtype also had a better prognosis than patients in the T2(HER2$^-$MIB$^-$CD3$^-$) subtype (**Fig. 5G**). Spearman correlation analysis revealed no correlation between patient subtypes T1(HER2$^+$MIB$^+$CD3$^+$) and T2(HER2$^-$MIB$^-$CD3$^-$) with HER2 IHC status or ISH gene amplification rate (Supplementary Table S5). Overall, these analyses demonstrate the correlation of these tumor-specific subtypes with survival and reveal their potential as a biomarker across trastuzumab therapy. Particularly, Spearman correlation analysis showed no correlation between any of these metabolites and HER2 protein (Supplementary Table S6). Moreover, multivariate analysis showed that HER2 did not show an independent prognostic value of either the T1(HER2$^+$MIB$^+$CD3$^+$) subtype [$P = 0.26$; HR, 0.68; 95% confidence interval (CI), 0.34–1.34] or the T2(HER2$^-$MIB$^-$CD3$^-$) subtype ($P = 0.26$; HR, 1.48; 95% CI, 0.75–2.93; Supplementary Table S7), further confirming that patient response to trastuzumab depends on tumor-specific subtype variables irrespective of HER2 expression.

Discussion

This study describes a novel tumor- and stroma-specific classification model in a large series of patients with gastric cancer based on metabolites. We defined three distinct tumor-specific subtypes: T1 (HER2$^+$MIB$^+$CD3$^+$), T2(HER2$^-$MIB$^-$CD3$^-$), and T3(pEGFR$^+$), and three stroma-specific subtypes: S1(FOXP3$^-$), S2(HER2$^-$MIB$^-$CD3$^-$) and S3(HER2$^+$MIB$^+$CD3$^+$FOXP3$^+$). The characteristics

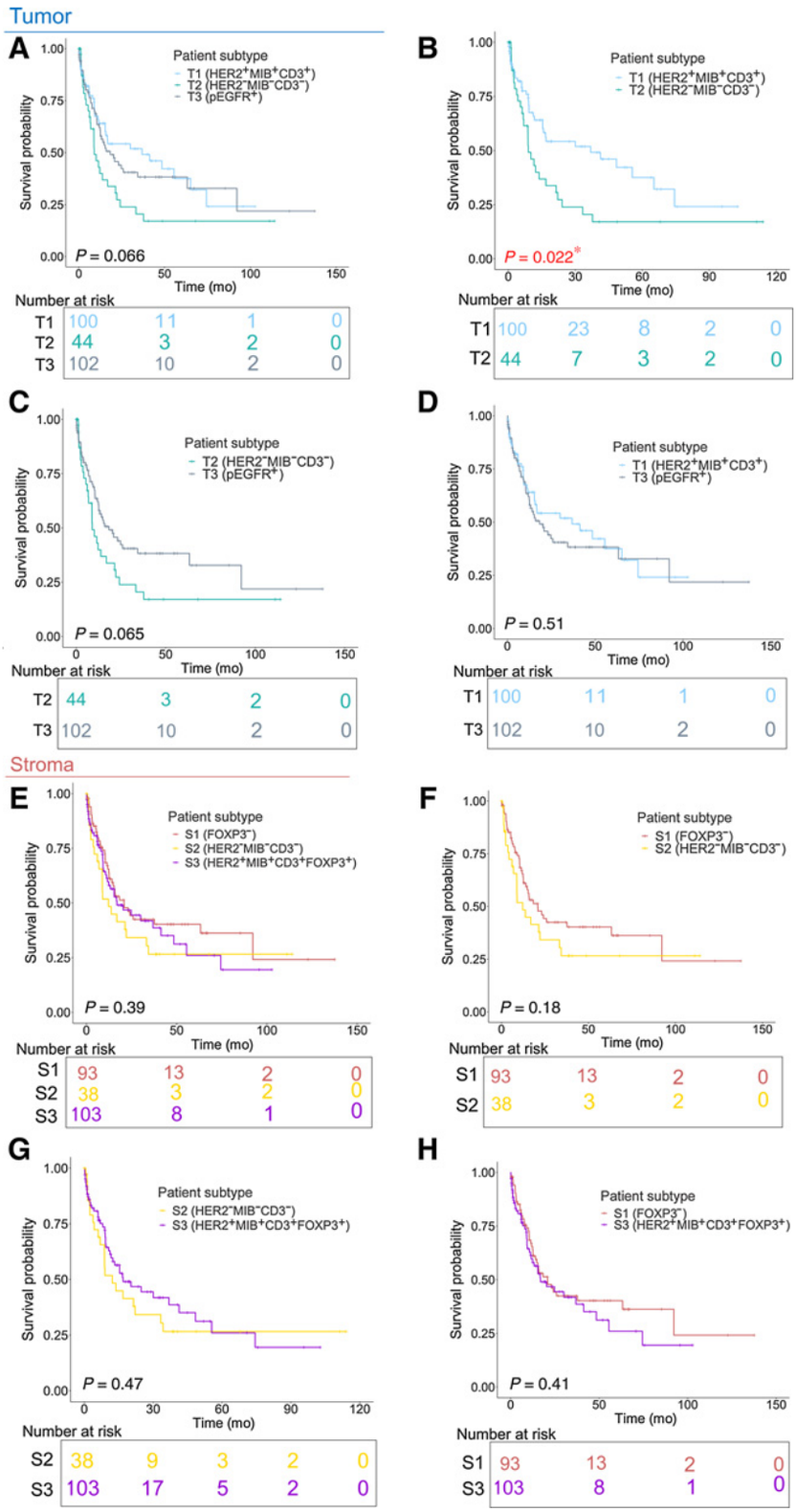

Figure 3.

Metabolic patient subtypes and their prognosis. Survival analysis of (**A**) three tumor-specific subtypes and (**B–D**) pairwise subtype comparison in Kaplan–Meier curves. Survival analysis of (**E**) three stroma-specific subtypes and (**F–H**) pairwise subtype comparison. The *x*-axis represented the survival time, and the *y*-axis represented the probability of survival. The log-rank test was used to assess the statistical significance of the prognostic differences among the subtypes; *, $P < 0.05$.

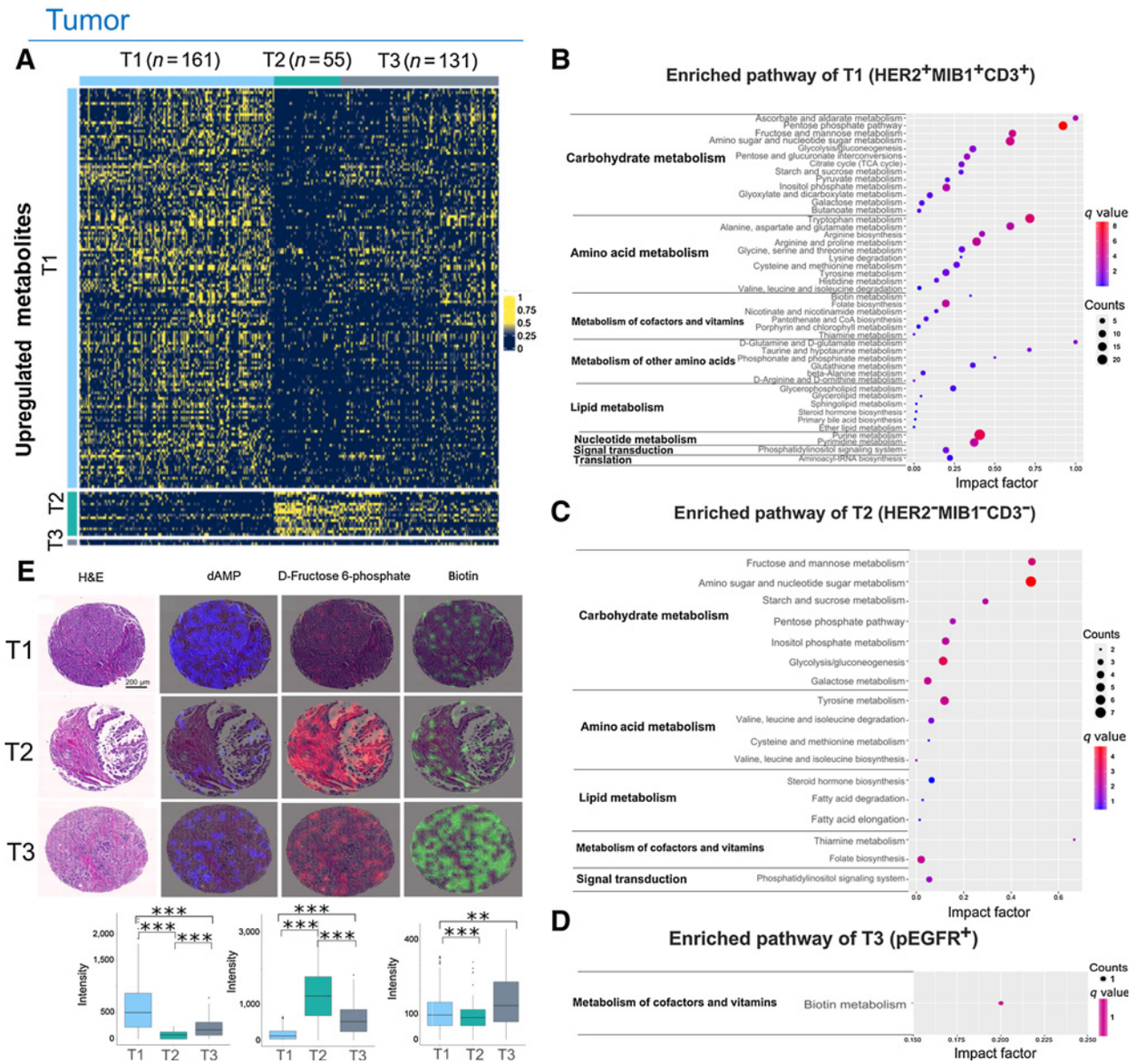

Figure 4.

Q7 Tumor subtype-specific metabolite characteristics and pathways enrichment. **A,** Upregulated metabolites of each tumor-specific subtype. Each row represented one metabolite. Colored bars at the top indicated tumor-specific subtypes. **B–D,** Pathways enriched in each tumor-specific subtype were represented by scatter plots. The *x*-axis indicated the pathway impact factor, and the *y*-axis indicated the pathway term. Dot color indicated the *q* value. Dot size indicated the counts of metabolites. **E,** Representative upregulated metabolite distribution and its intensities in the tumor-specific subtypes. Deoxyadenosine monophosphate (dAMP), a nucleotide metabolism member; D-Fructose 6-phosphate, carbohydrate metabolism member; Biotin, biotin metabolism member. The statistic differences were evaluated with the Kruskal–Wallis test; ***, $P < 0.001$.

of tumor-specific subtypes are summarized in **Fig. 6**. T1 ($HER2^+MIB^+CD3^+$) was characterized by high immune cell infiltration, presence of EBV, MSI-H, earlier UICC stage, nucleotide metabolism, and good prognosis. By contrast, T2($HER2^-MIB^-CD3^-$) was characterized by low immune cell infiltration, absence of EBV, low MSI, later UICC stage and poor prognosis; Finally, T3($pEGFR^+$) was characterized by high pEGFR. Stroma-specific subtypes were linked to distinct metabolic pathways and molecular features. An independent validation cohort confirmed that the T1($HER2^+MIB^+CD3^+$) subtype had predictive power for a trastuzumab benefit. Identification of these tumor- and stroma-specific subtypes would be a valuable addition to current molecular classification by maximizing the use of established therapy in proper patient populations and reducing the use of costly drugs.

In recent years, molecular methods, such as next-generation sequencing, including deoxyribonucleic acid sequencing, ribonucleic acid sequencing, whole-exome sequencing, copy-number variation analysis, and DNA methylation arrays, have been used for the classification of gastric cancer into molecular subtypes (7–10, 35). Our subtype classification drew from these stratification approaches and

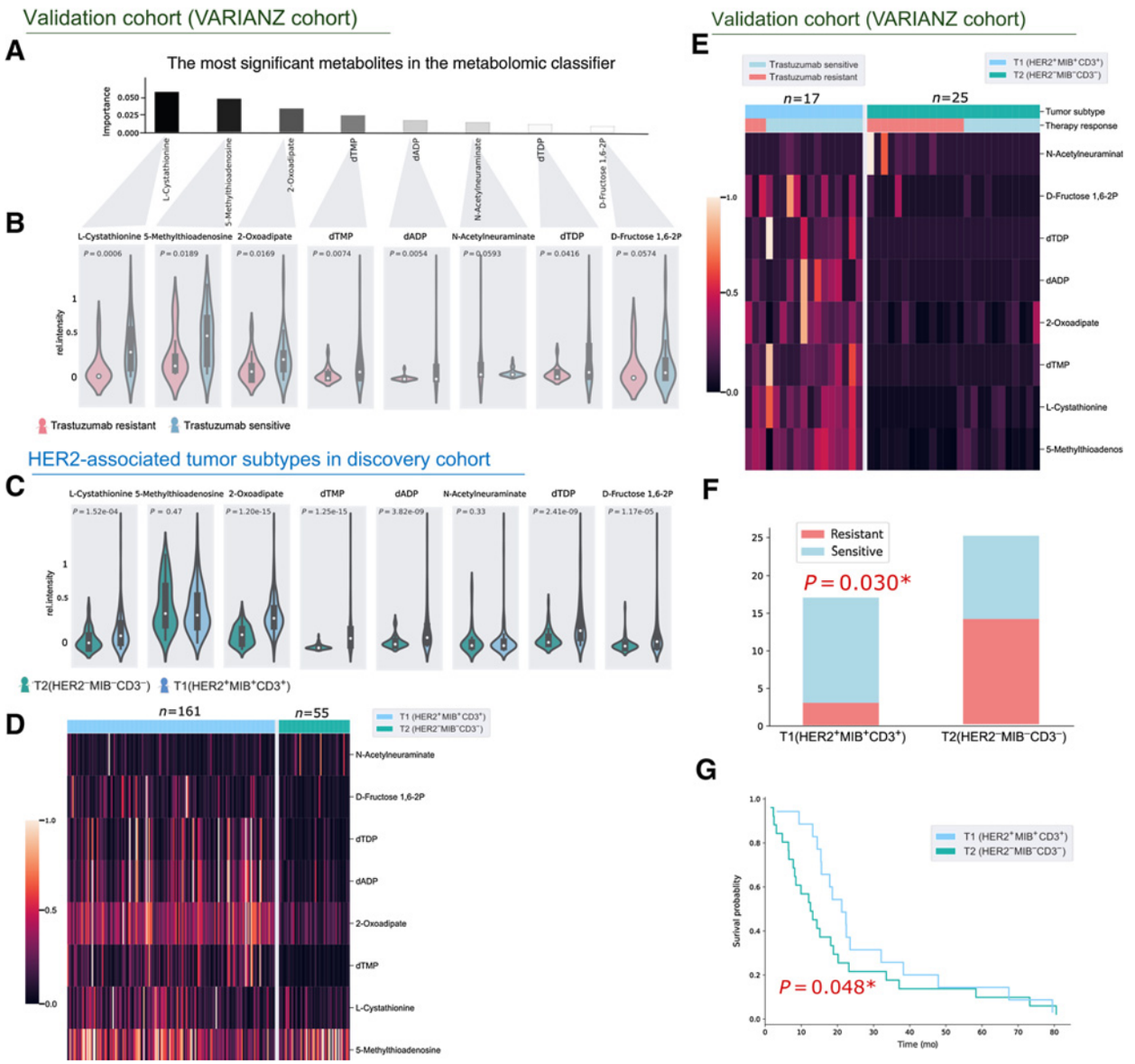

Figure 5.

Association with trastuzumab therapy response in HER2-associated tumor-specific subtypes T1(HER2$^+$MIB$^+$CD3$^+$) and T2(HER2$^-$MIB$^-$CD3$^-$). **A,** Importance plot, including the most significant metabolites, which represented an unequal distribution of trastuzumab-sensitive and -resistant patients in the metabolomic classifier from the VARIANZ cohort. **B,** Abundance difference of metabolites in trastuzumab-sensitive and trastuzumab-resistant patients with gastric cancer using the Mann–Whitney *U* test. **C,** The abundance difference of metabolites in T1(HER2$^+$MIB$^+$CD3$^+$) and T2(HER2$^-$MIB$^-$CD3$^-$) subtypes using the Mann–Whitney *U* test. **D,** Heatmap illustrating the abundance of metabolites showed tumor-specific subtype classification in our discovery cohort. **E,** Heatmap of the abundance of metabolites showed tumor-specific subtype classification in the VARIANZ cohort. **F,** Numbers of trastuzumab-sensitive and trastuzumab-resistant patients in T1(HER2$^+$MIB$^+$CD3$^+$) and T2(HER2$^-$MIB$^-$CD3$^-$) subtypes. The *P* value was calculated by using the Fisher's exact test. **G,** Survival difference of patients with T1(HER2$^+$MIB$^+$CD3$^+$) and T2 (HER2$^-$MIB$^-$CD3$^-$) subtypes treated with trastuzumab therapy using the log-rank test; *, $P < 0.05$.

supplemented them using tissue metabolomics to stratify patients with gastric cancer. The T1(HER2$^+$MIB$^+$CD3$^+$) subtype shared similarity to the EBV$^+$ and MSI subtypes established by TCGA study (7) for the presence of EBV and high MSI. The T2(HER2$^-$MIB$^-$CD3$^-$) subtype was similar to the ImD in immune cell absence and showed consistently poor survival (9). Good prognosis in T1(HER2$^+$MIB$^+$CD3$^+$) and poor prognosis in T2(HER2$^-$MIB$^-$CD3$^-$) subtypes may be due to the combined effects of high CD3, CD8, and FOXP3 expression. Previous studies support our observation that high T-cell density was associated with improved gastric cancer clinical outcomes (14, 36).

Only a subset of patients benefit from trastuzumab therapy (32). However, effective prediction of treatment response to trastuzumab could dramatically enhance this benefit ratio while preventing overtreatment. Several response predictors have been proposed. However, at present, neither HER2 IHC (11) nor HER2 ISH (37) provides a robust prediction of trastuzumab therapy benefit in patients with

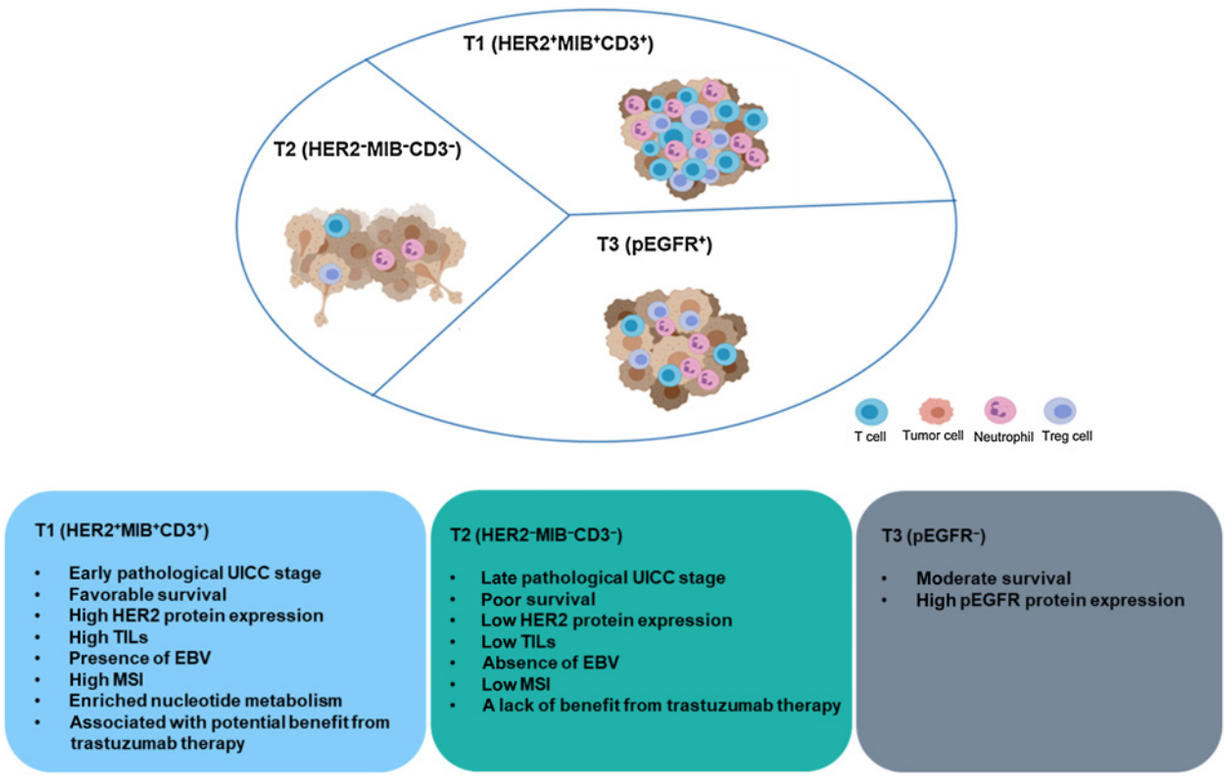

Figure 6.

Summary of clinicopathological and molecular characteristics of three tumor-specific gastric cancer patient subtypes. The three tumor-specific subtypes displayed significantly distinct metabolites and molecular features. Human Epidermal Growth Factor Receptor 2, HER2; tumor-infiltrating lymphocytes, TIL; Epstein–Barr Virus, EBV; Microsatellite Instability, MSI; phospho-Epidermal Growth Factor Receptor, pEGFR.

gastric cancer. Therefore, *a priori* identification of responders is critically needed as it would improve treatment outcomes. A metabolomic classifier involving DNA metabolism molecules was built in our previous study, and could predict trastuzumab response in patients with HER2-positive gastric cancer (31). Patients with HER2-positive tumor from this recent study were used as the validation cohort, and the same metabolomic classifier was applied in the current study. We successfully confirmed that our tumor-specific subtypes can further stratify HER2-positive patient responses to trastuzumab therapy, with patients with gastric cancer possessing T1($HER2^+MIB^+CD3^+$) experiencing better outcomes to trastuzumab therapy than T2 ($HER2^-MIB^-CD3^-$) patients. Strikingly, nucleotides were elevated in sensitive patients, and DNA metabolism in gastric cancer tumor cells has been reported as a crucial factor that affects the response to trastuzumab therapy in our previous study (31). The current study consistently showed a higher abundance of nucleotides and DNA metabolism in the T1 ($HER2^+MIB^+CD3^+$) subtype. Together, this evidence suggests that the T1($HER2^+MIB^+CD3^+$) subtype assignment predicts a benefit when initiating trastuzumab therapy.

In addition, response to trastuzumab therapy has been reported to improve when combined with bifunctional HER2/CD3 CART-like human T-cell treatment (38). Significant inhibition in drug-resistant solid tumors has been exhibited in other HER2-targeted bispecific antibodies undergoing clinical investigation, including ertumaxomab-targeting HER2 and CD3 on T cells and activated T-cell armed with HER2-targeted bispecific antibody (HER2Bi-aATC; ref. 39). In our study, HER2 and CD3 protein expressions were found to be positively correlated with the T1($HER2^+MIB^+CD3^+$) subtype. Hence, we expect the T1($HER2^+MIB^+CD3^+$) subtype to be predisposed with the trastuzumab therapy combined with HER2-targeted bispecific antibodies.

Pioneering studies in this field revealed a close correlation between TILs and PD-L1 overexpression in gastric cancer (16, 40). The expression of PD-1 is found not only on $CD8^+$-infiltrated cells but also on $FOXP3^+$ Treg cells (18). Tumors with elevated immune infiltration often have a more active response to immunotherapy (41). Patients with these characteristics had better clinical outcomes in response to immune checkpoint therapy. Thus, TILs can be considered a potentially important predictive marker in a broad variety of gastric cancer and other tumor types (14, 42). Some previous studies have demonstrated that PD-1 blockade could be effective in patients with elevated $CD8^+$ TILs, even with low PD-L1 expression (43–45). In addition, several recent studies found a close relationship of immune checkpoints with EBV-positive and MSI-high gastric cancer (14, 15). Thus, we expect T1($HER2^+MIB^+CD3^+$) to be predisposed with immune checkpoint inhibitors, such as PD-1 blockade, because of its higher frequency of EBV positivity, MSI and positive correlation with $CD8^+$ T-cell infiltration and FOXP3-positive Treg cells.

Immunotherapy has also been successfully added to HER2-directed therapy. The phase 3 KEYNOTE-811 trial recently showed that adding pembrolizumab to trastuzumab and chemotherapy markedly reduced tumor size, induced complete responses in some participants, and significantly improved objective response rate chemotherapy in HER2-positive, metastatic gastroesophageal adenocarcinoma (46). Notably, there was an impressive 74.4% response rate, which was

significantly higher than the 47% response rate achieved with chemotherapy plus trastuzumab, suggesting that T1(HER2$^+$MIB$^+$CD3$^+$) treatment responsiveness may be increased by combining checkpoint blockade with standard trastuzumab plus chemotherapy.

The distinct metabolite networks and biochemical processes in tumor- and stroma-specific subtypes revealed by enriched pathway analysis were consistent with previously known features of gastric cancer. For instance, previous studies suggested that metabolic alteration was typically characterized by repression of the Warburg effect aerobic respiration and increased glycolysis for glucose metabolism (19, 47, 48). The association between glucose metabolism and gastric cancer has been confirmed and discussed in several studies (19, 48). One proposed explanation why the Warburg effect is advantageous for tumor growth is that through increased glycolysis, glycolytic intermediates can funnel into anabolic side pathways to support de novo synthesis of nucleotides, lipids, and amino acids needed to support cell proliferation (47, 49). This evidence robustly supports our observation that carbohydrate metabolism and amino acid metabolism pathways are enriched among T1(HER2$^+$MIB$^+$CD3$^+$), T2(HER2$^-$MIB$^-$CD3$^-$), S2(HER2$^-$MIB$^-$CD3$^-$), and S3(HER2$^+$MIB$^+$CD3$^+$FOXP3$^+$) subtypes. Apart from commonly enriched metabolism, T1 (HER2$^+$MIB$^+$CD3$^+$) and S3(HER2$^+$MIB$^+$CD3$^+$FOXP3$^+$) specifically exhibited upregulation of nucleotide metabolism. Accumulation of nucleotide metabolism end products is also found in patients with gastric cancer (50).

Molecular expression profiles of tumor tissues may influence their assignment to specific molecular categories, creating interpretative challenges. Novel, distinctive, stroma-based signatures have been proposed for predominant cancer phenotypes (35). In this study, we successfully performed the classification of tumor epithelial cells and stromal cells, whereas no well-established large-scale classification research has considered the influence of active, nonmalignant stromal cells. As we found, T1(HER2$^+$MIB$^+$CD3$^+$) and S3(HER2$^+$MIB$^+$CD3$^+$FOXP3$^+$) share similar metabolic pathways but different correlations with pathological parameters and molecular features. This result shows that tumor- and stroma-specific metabolite patterns from the same patient may convey different information, and the same patient cohort may have different subtype patterns in tumor- and stroma-specific regions. Thus, identification of subtypes must be more precise to individual tumor or stroma regions rather than mixed tissue regions.

In conclusion, our results increase the understanding of the metabolic subtypes of gastric cancer. With the further development of image mass spectrometry tools, the metabolic classification of gastric cancer will become more precise. If confirmed and extended in future studies, the association between metabolic subtypes reported here and therapy responses might refine patient selection for personalized therapy.

Authors' Disclosures

F. Lordick reports grants, personal fees, and other support from BMS, as well as personal fees from Astra Zeneca, Astellas, Eli Lilly, MSD, Merck Serono, Roche, Amgen, Biontech, MedUpdate, StreamedUp!, and Novartis outside the submitted work. No disclosures were reported by the other authors.

Authors' Contributions

J. Wang: Conceptualization, formal analysis, visualization, methodology, writing–original draft, writing–review and editing. **T. Kunzke:** Conceptualization, methodology. **V.M. Prade:** Conceptualization, methodology. **J. Shen:** Visualization, writing–review and editing. **A. Buck:** Conceptualization, writing–review and editing. **A. Feuchtinger:** Methodology, writing–review and editing. **I. Haffner:** Resources, methodology, writing–review and editing. **B. Luber:** Methodology, writing–review and editing. **D.H.W. Liu:** Methodology, writing–review and editing. **R. Langer:** Methodology, writing–review and editing. **F. Lordick:** Resources, methodology, writing–review and editing. **N. Sun:** Conceptualization, resources, supervision, methodology, writing–review and editing. **A. Walch:** Conceptualization, resources, supervision, project administration, writing–review and editing.

Acknowledgments

The authors thank Ulrike Buchholz, Claudia-Mareike Pflüger, Cristina Hübner Freitas, Andreas Voss, and Elenore Samson for excellent technical assistance. The study was supported by the Ministry of Education and Research of the Federal Republic of Germany (BMBF; 01ZX1610B and 01KT1615; to A. Walch); the Deutsche Forschungsgmeinschaft SFB 824 C4, CRC/Transregio 205/1; to A. Walch); and the China Scholarship Council (CSC; No. 201906210076; to J. Wang).

The costs of publication of this article were defrayed in part by the payment of page charges. This article must therefore be hereby marked *advertisement* in accordance with 18 U.S.C. Section 1734 solely to indicate this fact.

Received December 14, 2021; revised March 1, 2022; accepted April 6, 2022; published first April 8, 2022.

References

1. Sung H, Ferlay J, Siegel RL, Laversanne M, Soerjomataram I, Jemal A, et al. Global cancer statistics 2020: GLOBOCAN estimates of incidence and mortality worldwide for 36 cancers in 185 countries. CA Cancer J Clin 2021;71:209–49.
2. Joshi SS, Badgwell BD. Current treatment and recent progress in gastric cancer. CA Cancer J Clin 2021;71:264–79.
3. Shah MA, Khanin R, Tang L, Janjigian YY, Klimstra DS, Gerdes H, et al. Molecular classification of gastric cancer: a new paradigm. Clin Cancer Res 2011; 17:2693–701.
4. Lin X, Zhao Y, Song WM, Zhang B. Molecular classification and prediction in gastric cancer. Comput Struct Biotechnol J 2015;13:448–58.
5. Lei Z, Tan IB, Das K, Deng N, Zouridis H, Pattison S, et al. Identification of molecular subtypes of gastric cancer with different responses to PI3-kinase inhibitors and 5-fluorouracil. Gastroenterology 2013;145: 554–65.
6. Liu Z, Zhang J, Gao Y, Pei L, Zhou J, Gu L, et al. Large-scale characterization of DNA methylation changes in human gastric carcinomas with and without metastasis. Clin Cancer Res 2014;20:4598–612.
7. Cancer Genome Atlas Research N. Comprehensive molecular characterization of gastric adenocarcinoma. Nature 2014;513:202–9.
8. Cristescu R, Lee J, Nebozhyn M, Kim KM, Ting JC, Wong SS, et al. Molecular analysis of gastric cancer identifies subtypes associated with distinct clinical outcomes. Nat Med 2015;21:449–56.
9. Li L, Wang X. Identification of gastric cancer subtypes based on pathway clustering. NPJ Precis Oncol 2021;5:46.
10. Zeng D, Li M, Zhou R, Zhang J, Sun H, Shi M, et al. Tumor microenvironment characterization in gastric cancer identifies prognostic and immunotherapeutically relevant gene signatures. Cancer Immunol Res 2019;7: 737–50.
11. Bang YJ, Van Cutsem E, Feyereislova A, Chung HC, Shen L, Sawaki A, et al. Trastuzumab in combination with chemotherapy versus chemotherapy alone for treatment of HER2-positive advanced gastric or gastro-oesophageal junction cancer (ToGA): a phase 3, open-label, randomised controlled trial. Lancet 2010; 376:687–97.
12. Muro K, Chung HC, Shankaran V, Geva R, Catenacci D, Gupta S, et al. Pembrolizumab for patients with PD-L1–positive advanced gastric cancer (KEYNOTE-012): a multicentre, open-label, phase 1b trial. Lancet Oncol 2016;17:717–26.
13. Fuchs CS, Doi T, Jang RW, Muro K, Satoh T, Machado M, et al. Safety and efficacy of pembrolizumab monotherapy in patients with previously treated

advanced gastric and gastroesophageal junction cancer: phase 2 clinical KEYNOTE-059 trial. JAMA Oncol 2018;4:e180013.
14. Dai C, Geng R, Wang C, Wong A, Qing M, Hu J, et al. Concordance of immune checkpoints within tumor immune contexture and their prognostic significance in gastric cancer. Mol Oncol 2016;10:1551–8.
15. Chao J, Fuchs CS, Shitara K, Tabernero J, Muro K, Van Cutsem E, et al. Assessment of pembrolizumab therapy for the treatment of microsatellite instability-high gastric or gastroesophageal junction cancer among patients in the KEYNOTE-059, KEYNOTE-061, and KEYNOTE-062 clinical trials. JAMA Oncol 2021;7:895–902.
16. Yi M, Jiao D, Xu H, Liu Q, Zhao W, Han X, et al. Biomarkers for predicting efficacy of PD-1/PD-L1 inhibitors. Mol Cancer 2018;17:129.
17. Kwon M, An M, Klempner SJ, Lee H, Kim KM, Sa JK, et al. Determinants of response and intrinsic resistance to PD-1 blockade in microsatellite instability-high gastric cancer. Cancer Discov 2021;11:2168–85.
18. Morihiro T, Kuroda S, Kanaya N, Kakiuchi Y, Kubota T, Aoyama K, et al. PD-L1 expression combined with microsatellite instability/CD8$^+$ tumor-infiltrating lymphocytes as a useful prognostic biomarker in gastric cancer. Sci Rep 2019;9:4633.
19. Yuan LW, Yamashita H, Seto Y. Glucose metabolism in gastric cancer: the cutting-edge. World J Gastroenterol 2016;22:2046–59.
20. Cluntun AA, Lukey MJ, Cerione RA, Locasale JW. Glutamine metabolism in cancer: understanding the heterogeneity. Trends Cancer 2017;3:169–80.
21. Huang S, Guo Y, Li Z, Zhang Y, Zhou T, You W, et al. A systematic review of metabolomic profiling of gastric cancer and esophageal cancer. Cancer Biol Med 2020;17:181–98.
22. Wei Q, Qian Y, Yu J, Wong CC. Metabolic rewiring in the promotion of cancer metastasis: mechanisms and therapeutic implications. Oncogene 2020;39:6139–56.
23. Andre F, Trinh A, Balayssac S, Maboudou P, Dekiouk S, Malet-Martino M, et al. Metabolic rewiring in cancer cells overexpressing the glucocorticoid-induced leucine zipper protein (GILZ): activation of mitochondrial oxidative phosphorylation and sensitization to oxidative cell death induced by mitochondrial targeted drugs. Int J Biochem Cell Biol 2017;85:166–74.
24. Peng X, Chen Z, Farshidfar F, Xu X, Lorenzi PL, Wang Y, et al. Molecular characterization and clinical relevance of metabolic expression subtypes in human Cancers. Cell Rep 2018;23:255–69.
25. Norris JL, Caprioli RM. Analysis of tissue specimens by matrix-assisted laser desorption/ionization imaging mass spectrometry in biological and clinical research. Chem Rev 2013;113:2309–42.
26. Ly A, Buck A, Balluff B, Sun N, Gorzolka K, Feuchtinger A, et al. High-mass-resolution MALDI mass spectrometry imaging of metabolites from formalin-fixed paraffin-embedded tissue. Nat Protoc 2016;11:1428–43.
27. Buck A, Ly A, Balluff B, Sun N, Gorzolka K, Feuchtinger A, et al. High-resolution MALDI-FT-ICR MS imaging for the analysis of metabolites from formalin-fixed, paraffin-embedded clinical tissue samples. J Pathol 2015;237:123–32.
28. Prade VM, Kunzke T, Feuchtinger A, Rohm M, Luber B, Lordick F, et al. De novo discovery of metabolic heterogeneity with immunophenotype-guided imaging mass spectrometry. Mol Metab 2020;36:100953.
29. Sobin LHGM, Wittekind C. TNM classification of malignant tumors. 7th ed. Oxford: Wiley-Blackwell; 2009.
30. Bosman FT, World Health Organization, International Agency for Research on Cancer. WHO classification of tumours of the digestive system. Lyon: International Agency for Research on Cancer; 2010. p. 417.
31. Kunzke T, Holzl FT, Prade VM, Buck A, Huber K, Feuchtinger A, et al. Metabolomic therapy response prediction in pretherapeutic tissue biopsies for trastuzumab in patients with HER2-positive advanced gastric cancer. Clin Transl Med 2021;11:e547.
32. Haffner I, Schierle K, Raimundez E, Geier B, Maier D, Hasenauer J, et al. HER2 expression, test deviations, and their impact on survival in metastatic gastric cancer: results from the Prospective Multicenter VARIANZ Study. J Clin Oncol 2021;39:1468–78.
33. Genitsch V, Novotny A, Seiler CA, Kroll D, Walch A, Langer R. Epstein-barr virus in gastro-esophageal adenocarcinomas—single center experiences in the context of current literature. Front Oncol 2015;5:73.
34. Berezowska S, Novotny A, Bauer K, Feuchtinger A, Slotta-Huspenina J, Becker K, et al. Association between HSP90 and Her2 in gastric and gastroesophageal carcinomas. PLoS One 2013;8:e69098.
35. Ren Q, Zhu P, Zhang H, Ye T, Liu D, Gong Z, et al. Identification and validation of stromal-tumor microenvironment-based subtypes tightly associated with PD-1/PD-L1 immunotherapy and outcomes in patients with gastric cancer. Cancer Cell Int 2020;20:92.
36. Arigami T, Uenosono Y, Ishigami S, Matsushita D, Hirahara T, Yanagita S, et al. Decreased density of CD3$^+$ tumor-infiltrating lymphocytes during gastric cancer progression. J Gastroenterol Hepatol 2014;29:1435–41.
37. Gomez-Martin C, Plaza JC, Pazo-Cid R, Salud A, Pons F, Fonseca P, et al. Level of HER2 gene amplification predicts response and overall survival in HER2-positive advanced gastric cancer treated with trastuzumab. J Clin Oncol 2013;31:4445–52.
38. Luo F, Qian J, Yang J, Deng Y, Zheng X, Liu J, et al. Bifunctional alphaHER2/CD3 RNA-engineered CART-like human T cells specifically eliminate HER2(+) gastric cancer. Cell Res 2016;26:850–3.
39. Yu S, Li A, Liu Q, Yuan X, Xu H, Jiao D, et al. Recent advances of bispecific antibodies in solid tumors. J Hematol Oncol 2017;10:155.
40. Thompson ED, Zahurak M, Murphy A, Cornish T, Cuka N, Abdelfatah E, et al. Patterns of PD-L1 expression and CD8 T-cell infiltration in gastric adenocarcinomas and associated immune stroma. Gut 2017;66:794–801.
41. Haanen J. Converting cold into hot tumors by combining immunotherapies. Cell 2017;170:1055–6.
42. Motz GT, Coukos G. Deciphering and reversing tumor immune suppression. Immunity 2013;39:61–73.
43. Sun JY, Zhang D, Wu S, Xu M, Zhou X, Lu XJ, et al. Resistance to PD-1/PD-L1 blockade cancer immunotherapy: mechanisms, predictive factors, and future perspectives. Biomark Res 2020;8:35.
44. Tumeh PC, Harview CL, Yearley JH, Shintaku IP, Taylor EJ, Robert L, et al. PD-1 blockade induces responses by inhibiting adaptive immune resistance. Nature 2014;515:568–71.
45. Nowicki TS, Hu-Lieskovan S, Ribas A. Mechanisms of resistance to PD-1 and PD-L1 blockade. Cancer J 2018;24:47–53.
46. Janjigian YY, Kawazoe A, Yanez P, Li N, Lonardi S, Kolesnik O, et al. The KEYNOTE-811 trial of dual PD-1 and HER2 blockade in HER2-positive gastric cancer. Nature 2021;600:727–30.
47. Vander Heiden MG, Cantley LC, Thompson CB. Understanding the Warburg effect: the metabolic requirements of cell proliferation. Science 2009;324:1029–33.
48. Leiting JL, Grotz TE. Advancements and challenges in treating advanced gastric cancer in the West. World J Gastrointest Oncol 2019;11:652–64.
49. Vander Heiden MG, DeBerardinis RJ. Understanding the intersections between metabolism and cancer biology. Cell 2017;168:657–69.
50. Yu L, Aa J, Xu J, Sun M, Qian S, Cheng L, et al. Metabolomic phenotype of gastric cancer and precancerous stages based on gas chromatography time-of-flight mass spectrometry. J Gastroenterol Hepatol 2011;26:1290–7.

AUTHOR QUERIES

AUTHOR PLEASE ANSWER ALL QUERIES

Q1: Page: 1: Author: Per journal style, genes, alleles, loci, and oncogenes are italicized; proteins are roman. Please check throughout to see that the words are styled correctly. AACR journals have developed explicit instructions about reporting results from experiments involving the use of animal models as well as the use of approved gene and protein nomenclature at their first mention in the manuscript. Please review the instructions at http://aacrjournals.org/content/authors/editorial-policies#genenomen to ensure that your article is in compliance. If your article is not in compliance, please make the appropriate changes in your proof.

Q2: Page: 1: Author: Please verify the drug names and their dosages used in the article.

Q3: Page: 1: Author: Please verify the affiliations and their corresponding author links.

Q4: Page: 1: Author: Please verify the corresponding author details.

Q5: Page: 3: Author: Please verify the layout of Tables for correctness.

Q6: Page: 5: Author: Please confirm quality/labeling of all images included within this article. Thank you.

Q7: Page: 9: Author: Please specify the significance of "**" appearing in the artwork of Fig. 4.

Q8: Page: 12: Author: The Authors' Disclosures statement that appears in the proof incorporates the information from forms completed and signed off on by each individual author. No factual changes can be made to disclosure information at the proof stage. However, typographical errors or misspelling of author names should be noted on the proof and will be corrected before publication. Please note if any such errors need to be corrected. Is the disclosure statement correct?

Q9: Page: 12: Author: The contribution(s) of each author are listed in the proof under the heading "Authors' Contributions." These contributions are derived from forms completed and signed off on by each individual author. If you make changes to these contributions, you must inform the affected author(s).

Q10: Page: 13: Author: Please provide complete details for Ref. 30.

AU: Below is a summary of the name segmentation for the authors according to our records. The First Name and the Surname data will be provided to PubMed when the article is indexed for searching. Please check each name carefully and verify that the First Name and Surname are correct. If a name is not segmented correctly, please write the correct First Name and Surname on this page and return it with your proofs. If no changes are made to this list, we will assume

that the names are segmented correctly, and the names will be indexed as is by PubMed and other indexing services.

First Name	Surname
Jun	Wang
Thomas	Kunzke
Verena M.	Prade
Jian	Shen
Achim	Buck
Annette	Feuchtinger
Ivonne	Haffner
Birgit	Luber
Drolaiz H.W.	Liu
Rupert	Langer
Florian	Lordick
Na	Sun
Axel	Walch